III European Conference on Computational Mechanics
Solids, Structures and Coupled Problems in Engineering
C.A. Mota Soares et.al. (eds.)
Lisbon, Portugal, 5–8 June 2006

DAMAGE LOCALIZATION IN LAMINATED COMPOSITE PLATES USING DOUBLE PULSE-ELECTRONIC HOLOGRAPHIC INTERFEROMETRY

J.V. Araújo dos Santos[1], H.M.R. Lopes[2], M. Vaz[3], C.M. Mota Soares[1], C.A. Mota Soares[1], and M.J.M. de Freitas[4]

[1]IDMEC/IST, Instituto Superior Técnico
Av. Rovisco Pais, 1049-001 Lisboa, Portugal
jsantos@dem.ist.utl.pt
cmmsoares@alfa.ist.utl.pt
carlosmotasoares@dem.ist.utl.pt

[2]ESTIG - Instituto Politécnico de Bragança
Campus de Sta Apolónia, Apartado 134, 5301-857 Bragança, Portugal
hlopes@ipb.pt

[3]DEMEGI - Faculdade de Engenharia do Porto
Rua Dr. Roberto Frias, 4200-465 Porto, Portugal
gmavaz@fe.up.pt

[4]ICEMS/UME, Instituto Superior Técnico
Av. Rovisco Pais, 1049-001 Lisboa, Portugal
mfreitas@dem.ist.utl.pt

Keywords: Damage Localization, Laminated Plate, Mode Shape Curvature, Double Pulse-Electronic Holographic Interferometry, Acoustic Excitation, Non Destructive Inspection.

Abstract. *One method for the damage localization of impact damage in laminated composite plates, based on their vibrational characteristics, is presented in this paper. This method uses double pulse-electronic holographic interferometry for mode shapes acquisition and the differences in curvatures. The rotations and curvatures are numerically obtained. The method is applied to a carbon fibre reinforced epoxy rectangular plate, free in space, subjected to two cases of impact damage. It is shown that the method based on curvatures allows for the localization of both cases of damage, which can be undetected by visual, X-ray or C-Scan inspections. The best localizations are achieved by selecting and applying the method to the most changed mode.*

1 INTRODUCTION

In recent years the use of laminated composite materials in many mechanical and aerospace engineering structures has seen a huge increase, due, among other factors, to their specific stiffness and strength. However, because of these materials characteristics, damage can be produced during fabrication or by inappropriate or hazardous service loads. Delamination is one the most common and dangerous damages, caused by internal failure of the laminas interface. These internal damages can be undetected by visual inspection. Therefore, in order to assess the structure integrity, non destructive inspection methods are needed for damage localization. The most used non destructive inspection methods are either visual or localized experimental methods such as acoustic or ultrasonic methods, magnet field methods, radiographs, eddy-current methods and thermal field methods [1]. These experimental methods can detect damage on or near the surface of the structure [1], therefore not allowing the detection of delaminations.

The use of vibration based delamination identification and health monitoring techniques for composite structures have been surveyed by Zou *et al.* [2]. The level of success in identifying damage is directly related to the sensitivity of the applied measurement technique and the parameters used in the identification methodology. Abdo and Hori [3], showed numerically that damage localization by mode shapes can be more easily accomplished if rotation differences are involved. However, in the presence of small defects with noisy data, obtained from experimental measurement, the use of rotations can mislead the damage localization. In these cases, a higher sensitivity parameter, like the curvature or strain energy, could be used instead [4, 5].

One method for the damage localization of impact damage in laminated composite plates, based on mode shapes curvature differences, is presented, applied and discussed in this paper. The measurement of mode shapes translations is performed using double pulse-electronic holographic interferometry and the plate is excited acoustically. In order to overcome the problem of differentiating noisy data, the rotations and curvatures are obtained by numerical differentiation of modes shapes translations using a differentiation/smoothing technique [6, 7, 8, 9, 10, 11].

The proposed methodology was applied to a carbon fiber reinforced epoxy rectangular plate, free in space, subjected to two cases of impact damage. The results of applying the mentioned method showed that the curvature differences allow the localization of both cases of damage, which can be undetected by visual, standard X-ray or C-Scan inspections. Finally, it was also found that the best localizations are achieved by selecting the most changed mode, due to the presence of damage.

2 EXPERIMENTAL SETUP

A carbon fiber reinforced epoxy rectangular plate, with a $[0/90/+45/-45/0/90]_{\mathrm{s}}$ stacking sequence, was analyzed before and after being damaged by impact using the experimental techniques described in this Section. The plate in-plane dimensions are 277.0 mm $\times$ 199.0 mm and its thickness is 1.80 mm. The specific mass is $\rho = 1562$ kg/m^3 and the laminas mechanical properties are $E_1 = 123.4$ GPa, $E_2 = 8.6$ GPa, $G_{12} = G_{13} = 5.0$ GPa, $G_{23} = 6.1$ GPa, $\nu_{12} = 0.14$, which were obtained using a technique described in [12]. The first ten natural frequencies of the plate were obtained from its Frequency Response Functions (FRFs). The plate was suspended with high flexible rubber bands creating a nearly free condition. A transient excitation was performed with an impact hammer *Brüel & Kjær* model 8203 and a non contact measurement of the plate response was carried out with a microphone. Both signals were processed in a *Brüel & Kjær* analyzer, model 2148. In Figure 1 is shown a view of the setup used.

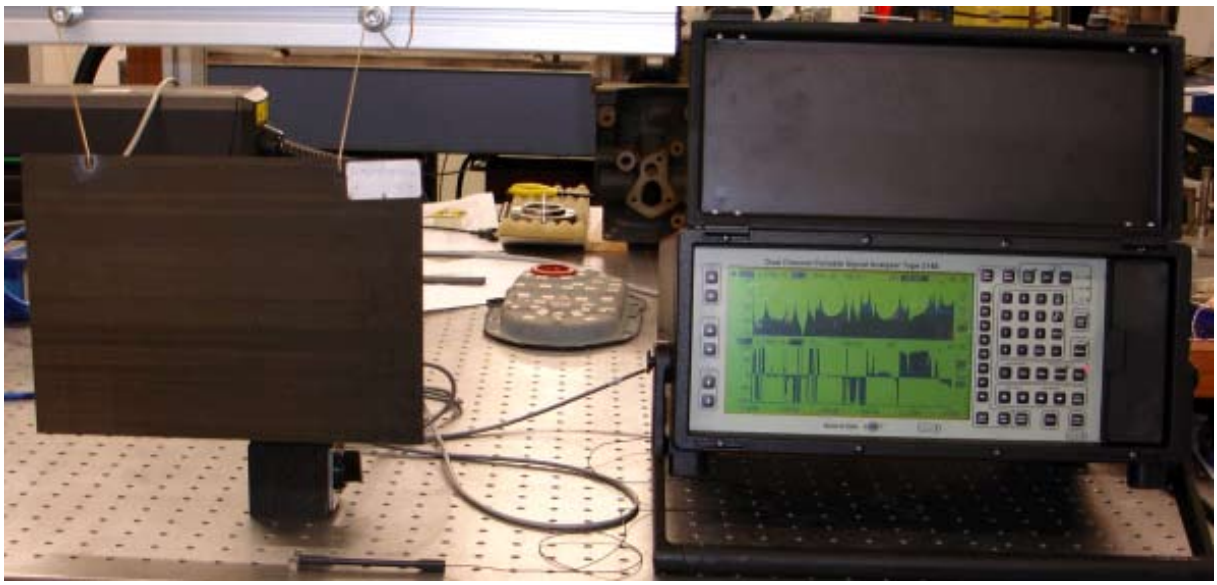

Figure 1: Experimental setup for Frequency Response Functions measurements.

A double pulse-electronic holographic interferometry set up with acoustic excitation was used to assess the plate mode shapes. This high sensitive technique allows a non contact measurement of the mode shapes with no influence in the plate mass distribution. A double-pulsed Ruby Laser was used to generate pairs of pulses with a time separation varying between 1μs and 800μs. The double pulse speckle patterns were recorded with an asynchronous CCD camera, with a 512×512 resolution (Figures 2 and 3).

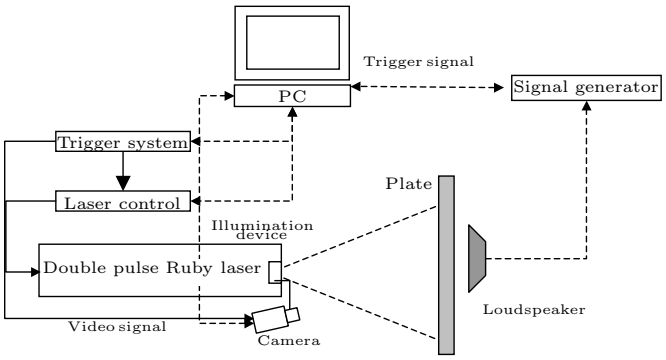

Figure 2: Schematic of experimental setup for mode shapes measurements.

To assess the phase map of each speckle pattern a spatial carrier is introduced in the primary fringes by a small tilt in the reference wave front [13]. Due to the short time between recordings, any low frequency rigid body movement of the plate is eliminated. The two interferograms are post-processed using dedicated image processing techniques [7, 10, 11, 14, 15, 16, 17, 18, 19] and thus the mode shapes translations are obtained.

The spatial differentiation of these mode shapes translations was carried out by combining smoothing/differentiation techniques. The procedure used is very simple and allows high quality results [9], relatively to other numerical differentiation techniques, such as finite differences.

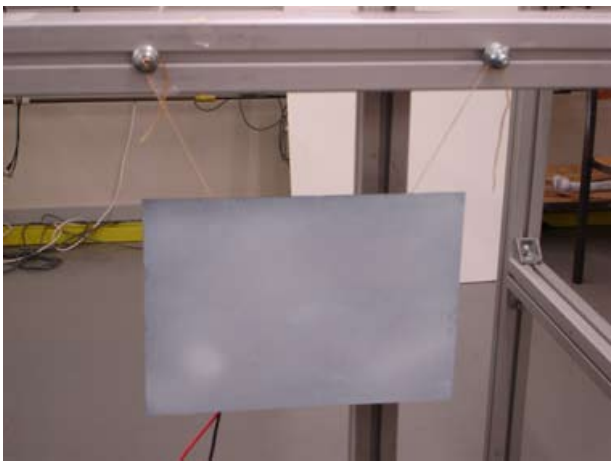

(a) Laminated test plate

(b) Ruby Laser LUMONICS and CCD camera

(c) Excitation loudspeaker

Figure 3: Experimental setup for mode shapes measurements.

Between each evaluation a smoothing algorithm is applied [7]. Figures 4 and 5 show the undamaged plate fringe patterns, translations and rotations of the first and tenth mode shapes, respectively.

3 DAMAGE LOCALIZATION METHOD

Consider the kth point, with (x, y) coordinates, and the ith mode shape of a plate. Let their undamaged and damaged out-of-plane translations be defined as

$$w_{ki} \quad \text{and} \quad \widetilde{w}_{ki}. \tag{1}$$

The rotation, $\boldsymbol{\theta}_{ki}$ and $\widetilde{\boldsymbol{\theta}}_{ki}$, and curvature, $\boldsymbol{\kappa}_{ki}$ and $\widetilde{\boldsymbol{\kappa}}_{ki}$, vectors can be defined in terms of these

(a) Fringe patterns

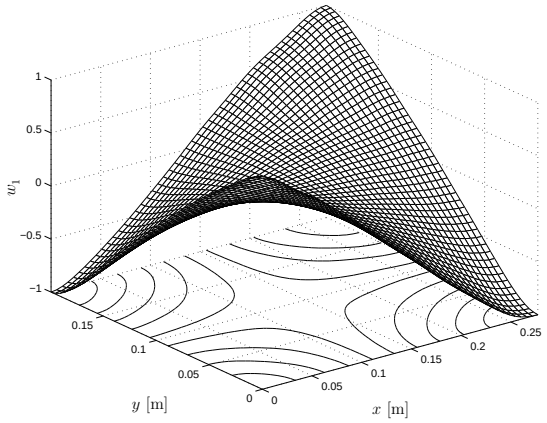

(b) Translations w

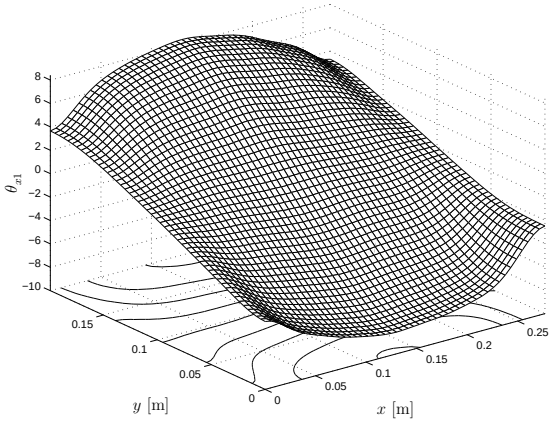

(c) Rotations θ_x

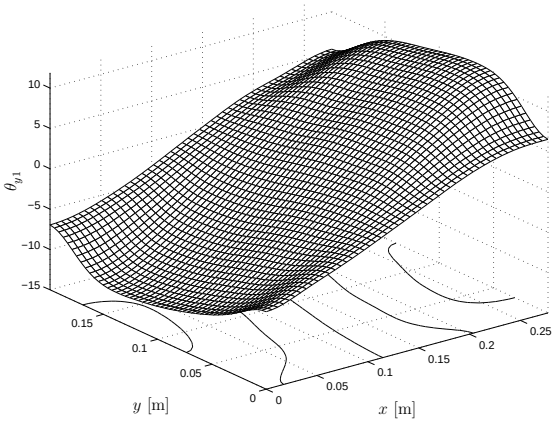

(d) Rotations θ_y

Figure 4: Undamaged plate first mode shape ($f_1 = 95.0$ Hz).

translations by

$$\begin{aligned} \boldsymbol{\theta}_{ki} &= \left\{ (\theta_x)_{ki}, (\theta_y)_{ki} \right\}^T = \left\{ \frac{\partial w_{ki}}{\partial x}, \frac{\partial w_{ki}}{\partial y} \right\}^T, \\ \widetilde{\boldsymbol{\theta}}_{ki} &= \left\{ \left(\widetilde{\theta}_x\right)_{ki}, \left(\widetilde{\theta}_y\right)_{ki} \right\}^T = \left\{ \frac{\partial \widetilde{w}_{ki}}{\partial x}, \frac{\partial \widetilde{w}_{ki}}{\partial y} \right\}^T \end{aligned} \tag{2}$$

and

$$\begin{aligned} \boldsymbol{\kappa}_{ki} &= \left\{ -\frac{\partial^2 w_{ki}}{\partial x^2}, -\frac{\partial^2 w_{ki}}{\partial y^2}, -2\frac{\partial^2 w_{ki}}{\partial x \partial y} \right\}^T, \\ \widetilde{\boldsymbol{\kappa}}_{ki} &= \left\{ -\frac{\partial^2 \widetilde{w}_{ki}}{\partial x^2}, -\frac{\partial^2 \widetilde{w}_{ki}}{\partial y^2}, -2\frac{\partial^2 \widetilde{w}_{ki}}{\partial x \partial y} \right\}^T. \end{aligned} \tag{3}$$

One can define the differences between curvatures, $CD\left(\boldsymbol{\kappa}_k, \widetilde{\boldsymbol{\kappa}}_k\right)$, in the kth point as follows:

$$CD\left(\boldsymbol{\kappa}_k, \widetilde{\boldsymbol{\kappa}}_k\right) = \frac{1}{n} \sum_i \mid \|\boldsymbol{\kappa}_{ki}\|_2 - \|\widetilde{\boldsymbol{\kappa}}_{ki}\|_2 \mid, \tag{4}$$

where $\|\boldsymbol{\kappa}_{ki}\|_2$, $\|\widetilde{\boldsymbol{\kappa}}_{ki}\|_2$ are the Euclidean norms of vectors $\boldsymbol{\kappa}_{ki}$ and $\widetilde{\boldsymbol{\kappa}}_{ki}$, respectively. The number of included mode shapes is denoted by n, while index i in expression (4) makes reference to the

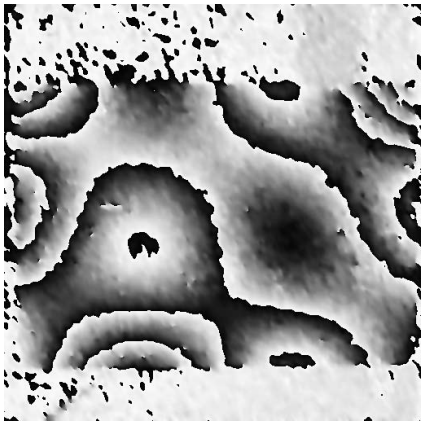

(a) Fringe patterns

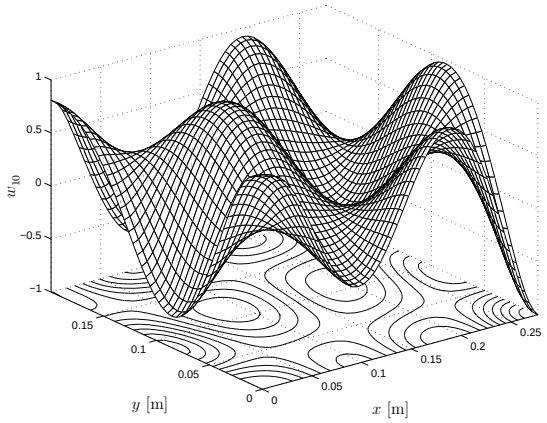

(b) Translations w

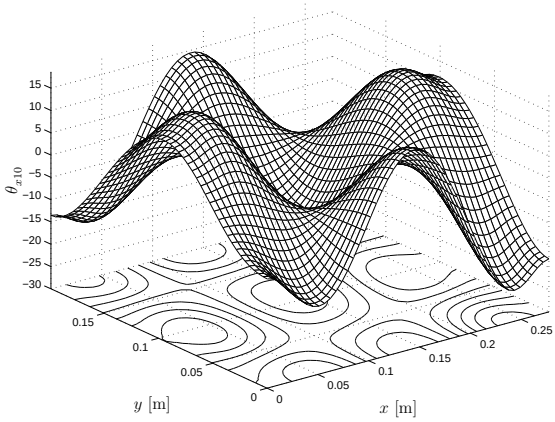

(c) Rotations θ_x

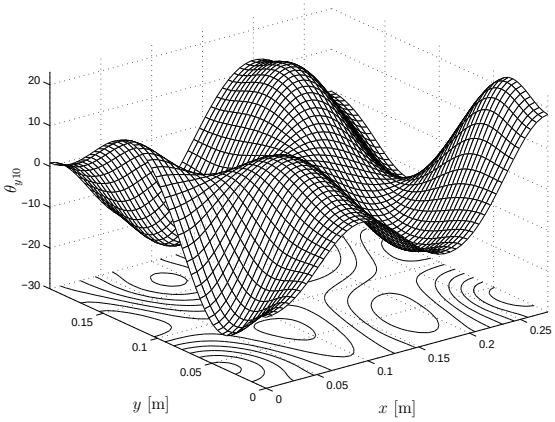

(d) Rotations θ_y

Figure 5: Undamaged plate tenth mode shape ($f_{10} = 770.5$ Hz).

chosen mode shape included in the computation of $CD\left(\boldsymbol{\kappa}_k, \widetilde{\boldsymbol{\kappa}}_k\right)$. In what follows, the method defined by expression (4) will be referred as Curvature Differences method.

4 APPLICATIONS

The plate presented in Section 2 was subjected to two cases of damage. The first case corresponds to a damage generated by a low energy impact in the center of the plate (Figure 6(a)), by dropping a steel ball. After measuring the natural frequencies and mode shapes, using the procedures described in Section 2, a second damaged was introduced in the plate by percuting the plate right upper corner (Figure 6(b)) with a rounded steel tip hammer and again the natural frequencies and mode shapes were measured.

Table 1 presents the percentual differences between the natural frequencies in the undamaged state (original natural frequencies) and the natural frequencies for both cases of damage (damaged natural frequencies). The numerical superscripts in Table 1 denote the case of damage and the values of FD are given by

$$FD\left(f_i, {}^1\widetilde{f}_i\right) = \frac{f_i - {}^1\widetilde{f}_i}{f_i} \times 100 \quad \text{and} \quad FD\left(f_i, {}^2\widetilde{f}_i\right) = \frac{f_i - {}^2\widetilde{f}_i}{f_i} \times 100.$$

The mode shapes were quantitatively compared using the modified Modal Assurance Crite-

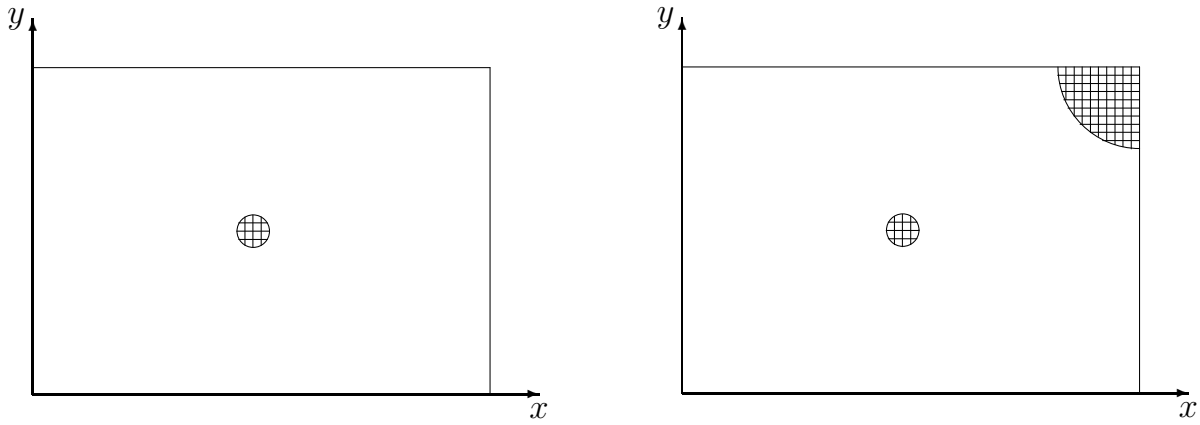

(a) Damage case 1 (b) Damage case 2

Figure 6: Schematic of impacted areas.

Modo i	f_i [Hz]	${}^1\widetilde{f}_i$ [Hz]	$FD\left(f_i, {}^1\widetilde{f}_i\right)$ [%]	${}^2\widetilde{f}_i$ [Hz]	$FD\left(f_i, {}^2\widetilde{f}_i\right)$ [%]
1	95.0	95.0	0.00	96.0	-1.05
2	158.5	158.0	0.32	158.5	0.00
3	248.0	247.0	0.40	247.5	0.20
4	263.0	262.5	0.19	262.5	0.19
5	321.5	322.5	-0.31	321.0	0.16
6	440.5	438.5	0.45	438.0	0.57
7	488.0	486.0	0.41	483.5	0.92
8	526.5	525.5	0.19	524.5	0.38
9	721.0	718.0	0.42	716.0	0.69
10	770.5	766.5	0.52	758.0	1.62

Table 1: Differences between original and damaged natural frequencies

rion (MAC) and the Normalized Modal Difference (NMD) parameters defined by

$$MAC\left(\mathbf{w}_i, \widetilde{\mathbf{w}}_i\right) = \frac{\left|\left(\mathbf{w}_i\right)^T \left(\widetilde{\mathbf{w}}_i\right)\right|^2}{\left[\left(\mathbf{w}_i\right)^T \left(\mathbf{w}_i\right)\right]\left[\left(\widetilde{\mathbf{w}}_i\right)^T \left(\widetilde{\mathbf{w}}_i\right)\right]} \quad \text{for} \quad 0 < MAC\left(\mathbf{w}_i, \widetilde{\mathbf{w}}_i\right) \leqslant 1,$$

$$NMD\left(\mathbf{w}_i, \widetilde{\mathbf{w}}_i\right) = \sqrt{\frac{1 - MAC\left(\mathbf{w}_i, \widetilde{\mathbf{w}}_i\right)}{MAC\left(\mathbf{w}_i, \widetilde{\mathbf{w}}_i\right)}} \quad \text{for} \quad 0 \leqslant NMD\left(\mathbf{w}_i, \widetilde{\mathbf{w}}_i\right) < \infty;$$

$$MAC\left(\boldsymbol{\theta}_{xi},\widetilde{\boldsymbol{\theta}}_{xi}\right)=\frac{\left|\left(\boldsymbol{\theta}_{xi}\right)^{T}\left(\widetilde{\boldsymbol{\theta}}_{xi}\right)\right|^{2}}{\left[\left(\boldsymbol{\theta}_{xi}\right)^{T}\left(\boldsymbol{\theta}_{xi}\right)\right]\left[\left(\widetilde{\boldsymbol{\theta}}_{xi}\right)^{T}\left(\widetilde{\boldsymbol{\theta}}_{xi}\right)\right]}\quad\text{for}\quad 0<MAC\left(\boldsymbol{\theta}_{xi},\widetilde{\boldsymbol{\theta}}_{xi}\right)\leqslant 1,$$

$$NMD\left(\boldsymbol{\theta}_{xi},\widetilde{\boldsymbol{\theta}}_{xi}\right)=\sqrt{\frac{1-MAC\left(\boldsymbol{\theta}_{xi},\widetilde{\boldsymbol{\theta}}_{xi}\right)}{MAC\left(\boldsymbol{\theta}_{xi},\widetilde{\boldsymbol{\theta}}_{xi}\right)}}\quad\text{for}\quad 0\leqslant NMD\left(\boldsymbol{\theta}_{xi},\widetilde{\boldsymbol{\theta}}_{xi}\right)<\infty;$$

$$MAC\left(\boldsymbol{\theta}_{yi},\widetilde{\boldsymbol{\theta}}_{yi}\right)=\frac{\left|\left(\boldsymbol{\theta}_{yi}\right)^{T}\left(\widetilde{\boldsymbol{\theta}}_{yi}\right)\right|^{2}}{\left[\left(\boldsymbol{\theta}_{yi}\right)^{T}\left(\boldsymbol{\theta}_{yi}\right)\right]\left[\left(\widetilde{\boldsymbol{\theta}}_{yi}\right)^{T}\left(\widetilde{\boldsymbol{\theta}}_{yi}\right)\right]}\quad\text{for}\quad 0<MAC\left(\boldsymbol{\theta}_{yi},\widetilde{\boldsymbol{\theta}}_{yi}\right)\leqslant 1,$$

$$NMD\left(\boldsymbol{\theta}_{yi},\widetilde{\boldsymbol{\theta}}_{yi}\right)=\sqrt{\frac{1-MAC\left(\boldsymbol{\theta}_{yi},\widetilde{\boldsymbol{\theta}}_{yi}\right)}{MAC\left(\boldsymbol{\theta}_{yi},\widetilde{\boldsymbol{\theta}}_{yi}\right)}}\quad\text{for}\quad 0\leqslant NMD\left(\boldsymbol{\theta}_{yi},\widetilde{\boldsymbol{\theta}}_{yi}\right)<\infty;$$

$$MAC\left(\mathbf{q}_{i},\widetilde{\mathbf{q}}_{i}\right)=\frac{\left|\left(\mathbf{q}_{i}\right)^{T}\left(\widetilde{\mathbf{q}}_{i}\right)\right|^{2}}{\left[\left(\mathbf{q}_{i}\right)^{T}\left(\mathbf{q}_{i}\right)\right]\left[\left(\widetilde{\mathbf{q}}_{i}\right)^{T}\left(\widetilde{\mathbf{q}}_{i}\right)\right]}\quad\text{for}\quad 0<MAC\left(\mathbf{q}_{i},\widetilde{\mathbf{q}}_{i}\right)\leqslant 1,$$

$$NMD\left(\mathbf{q}_{i},\widetilde{\mathbf{q}}_{i}\right)=\sqrt{\frac{1-MAC\left(\mathbf{q}_{i},\widetilde{\mathbf{q}}_{i}\right)}{MAC\left(\mathbf{q}_{i},\widetilde{\mathbf{q}}_{i}\right)}}\quad\text{for}\quad 0\leqslant NMD\left(\mathbf{q}_{i},\widetilde{\mathbf{q}}_{i}\right)<\infty,$$

where $\mathbf{w}_i$ e $\widetilde{\mathbf{w}}_i$, $\boldsymbol{\theta}_{xi}$ and $\widetilde{\boldsymbol{\theta}}_{xi}$, $\boldsymbol{\theta}_{yi}$ and $\widetilde{\boldsymbol{\theta}}_{yi}$ are, respectively, the partition vectors of the global vectors $\mathbf{q}_i=\left\{\mathbf{w}_i,\boldsymbol{\theta}_{xi},\boldsymbol{\theta}_{yi}\right\}$ and $\widetilde{\mathbf{q}}_i=\left\{\widetilde{\mathbf{w}}_i,\widetilde{\boldsymbol{\theta}}_{xi},\widetilde{\boldsymbol{\theta}}_{yi}\right\}$, relative to the translations and rotations about y and x axis, of the ith mode.

The values of MAC and NMD, presented in Tables 2 and 3, were obtained taking into account 481 components in the partition vectors and 1443 components in vectors $\mathbf{q}_i$ e $\widetilde{\mathbf{q}}_i$. Therefore, these vectors contain the translations and rotations in 481 points, schematically represented by black dots in Figure 7. The choice of these points was made in order to compare the experimental mode shapes with those numerically obtained, using a plate finite element model based on the first order shear deformation theory [12]. In Tables 2 and 3, the values of NMD greater than 50% and the corresponding MAC are printed in bold.

By comparing the values presented in Tables 1 with those in Tables 2 and 3, one can conclude that the most changed modes are not necessarily the ones with the biggest differences in natural frequencies. The most changed mode shapes translations for both cases of damage are presented in Figures 8 and 9, where are also shown the undamaged mode shapes translations.

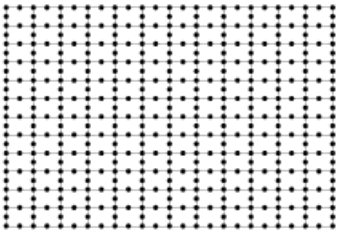

Figure 7: Distribution of points for the computation of MAC and NMD.

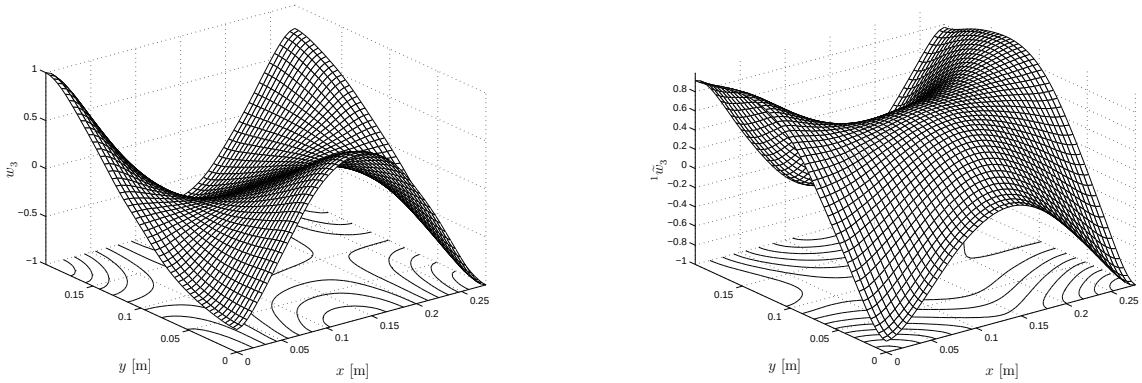

(a) Undamaged (b) Damage case 1

Figure 8: Third mode shape translations.

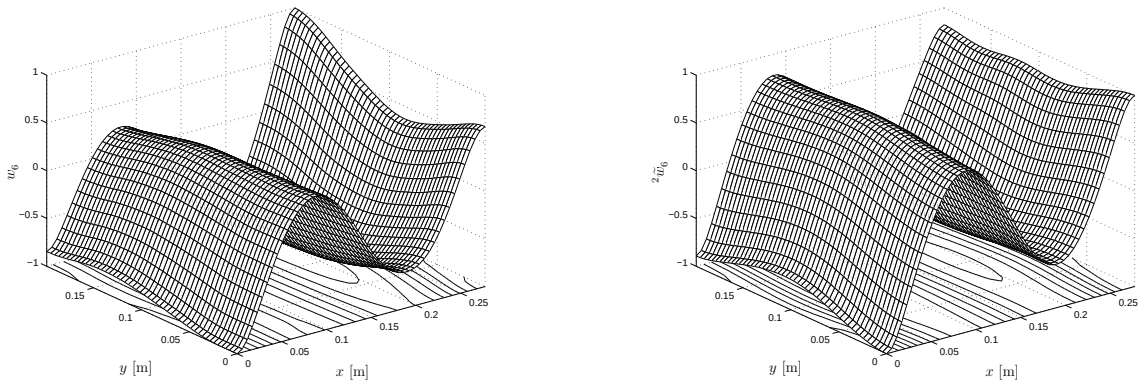

(a) Undamaged (b) Damage case 2

Figure 9: Sixth mode shape translations.

Modo i	1	2	3	4	5	6	7	8	9	10
f_i [Hz]	95.0	158.5	248.0	263.0	321.5	440.5	488.0	526.5	721.0	770.5
${}^1\widetilde{f}_i$ [Hz]	95.0	158.0	247.0	262.5	322.5	438.5	486.0	525.5	718.0	766.5
$MAC\left(\mathbf{w}_i, {}^1\widetilde{\mathbf{w}}_i\right)$	0.9892	0.9986	**0.1885**	0.9567	**0.7756**	0.8555	0.9833	0.9768	0.9493	0.9363
$NMD\left(\mathbf{w}_i, {}^1\widetilde{\mathbf{w}}_i\right)$ [%]	10.47	3.72	**207.50**	21.28	**53.78**	41.09	13.02	15.42	23.10	26.08
$MAC\left(\boldsymbol{\theta}_{xi}, {}^1\widetilde{\boldsymbol{\theta}}_{xi}\right)$	0.9843	0.9981	0.9733	0.8459	0.8723	0.9823	0.9895	0.9914	**0.7023**	0.9635
$NMD\left(\boldsymbol{\theta}_{xi}, {}^1\widetilde{\boldsymbol{\theta}}_{xi}\right)$ [%]	12.65	4.37	16.57	42.68	38.26	13.43	10.31	9.34	**65.10**	19.47
$MAC\left(\boldsymbol{\theta}_{yi}, {}^1\widetilde{\boldsymbol{\theta}}_{yi}\right)$	0.9918	0.9759	**0.0784**	0.9934	0.9732	**0.7051**	0.9931	0.9790	0.9882	0.8753
$NMD\left(\boldsymbol{\theta}_{yi}, {}^1\widetilde{\boldsymbol{\theta}}_{yi}\right)$ [%]	9.11	15.72	**342.90**	8.17	16.60	**64.67**	8.35	14.65	10.91	37.74
$MAC\left(\mathbf{q}_i, {}^1\widetilde{\mathbf{q}}_i\right)$	0.9893	0.9975	**0.2989**	0.9912	0.9612	0.9759	0.9916	0.9874	0.9782	0.9160
$NMD\left(\mathbf{q}_i, {}^1\widetilde{\mathbf{q}}_i\right)$ [%]	10.40	4.99	**153.15**	9.42	20.09	15.70	9.21	11.31	14.94	30.29

Table 2: Differences between original and damaged mode shapes (Damage case 1)

Modo i	1	2	3	4	5	6	7	8	9	10
f_i [Hz]	95.0	158.5	248.0	263.0	321.5	440.5	488.0	526.5	721.0	770.5
${}^2\widetilde{f}_i$ [Hz]	96.0	158.5	247.5	262.5	321.0	438.0	483.5	524.5	716.0	758.0
$MAC\left(\mathbf{w}_i, {}^2\widetilde{\mathbf{w}}_i\right)$	0.9426	0.9894	0.9466	0.9401	0.8822	**0.7130**	0.9498	0.9634	0.9796	0.8867
$NMD\left(\mathbf{w}_i, {}^2\widetilde{\mathbf{w}}_i\right)$ [%]	24.68	10.36	23.74	25.25	36.54	**63.45**	23.00	19.50	14.42	35.75
$MAC\left(\boldsymbol{\theta}_{xi}, {}^2\widetilde{\boldsymbol{\theta}}_{xi}\right)$	0.9689	0.9995	0.9982	**0.6941**	0.9424	0.9680	0.9570	0.9946	0.8708	0.9638
$NMD\left(\boldsymbol{\theta}_{xi}, {}^2\widetilde{\boldsymbol{\theta}}_{xi}\right)$ [%]	17.91	2.15	4.26	**66.39**	24.72	18.18	21.21	7.34	38.52	19.38
$MAC\left(\boldsymbol{\theta}_{yi}, {}^2\widetilde{\boldsymbol{\theta}}_{yi}\right)$	0.9894	**0.7445**	0.9419	0.9842	0.9848	**0.4012**	0.9756	0.9642	0.9909	0.9448
$NMD\left(\boldsymbol{\theta}_{yi}, {}^2\widetilde{\boldsymbol{\theta}}_{yi}\right)$ [%]	10.37	**58.58**	24.83	12.65	12.42	**122.17**	15.83	19.27	9.59	24.17
$MAC\left(\mathbf{q}_i, {}^2\widetilde{\mathbf{q}}_i\right)$	0.9824	0.9936	0.9797	0.9807	0.9799	0.9556	0.9662	0.9871	0.9890	0.9536
$NMD\left(\mathbf{q}_i, {}^2\widetilde{\mathbf{q}}_i\right)$ [%]	13.40	8.00	14.40	14.03	14.33	21.56	18.71	11.43	10.55	22.05

Table 3: Differences between original and damaged mode shapes (Damage case 2)

4.1 Proposed non destructive inspection methods

Damage localization using 10 mode shapes

The following damage localizations results were obtained using the first ten mode shapes, *i.e.*, considering $n = 10$ and $i = 1, ..., 10$ in expression (4).

By applying the Curvature Differences method, one can see that the greatest values of $CD\left(\boldsymbol{\kappa}_k, \widetilde{\boldsymbol{\kappa}}_k\right)$ appear in the right upper corner of the plate (Figure 10(b)), while the damage in the plate center is not located (Figure 10(a)).

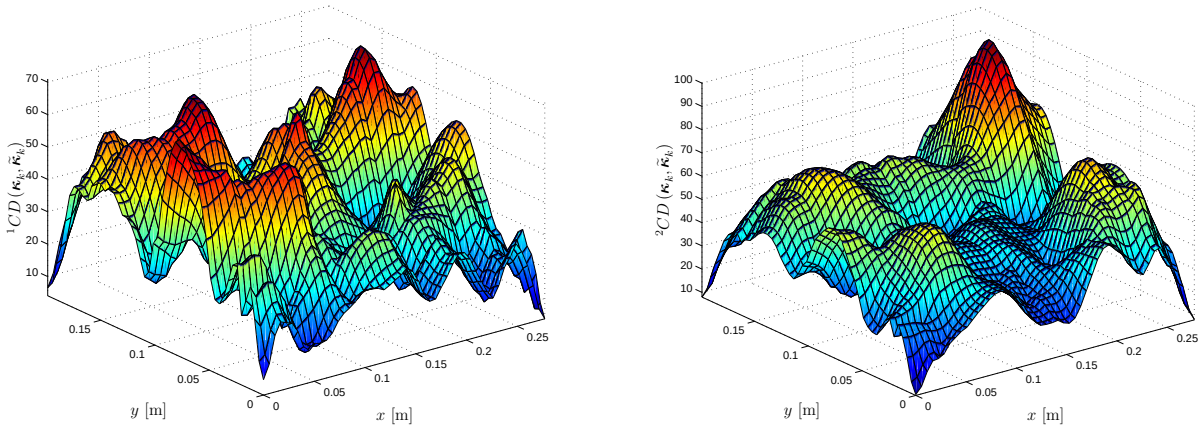

(a) Damage case 1 (b) Damage case 2

Figure 10: Damage localization with Curvature Differences method and 10 modes.

Damage localization using the most changed mode shape

Figures 11(a) and 11(b) present, respectively, a 3D plot and a contour plot of $CD\left(\boldsymbol{\kappa}_k, \widetilde{\boldsymbol{\kappa}}_k\right)$ values obtained by applying the Curvature Differences method to the most change mode shape, due to the damage in the plate center, *i.e.*, the third mode shape (see Table 2), by defining $n = 1$ and $i = 3$ in expression (4). The corresponding undamaged and damage natural frequencies are, respectively, $f_3 = 248$ Hz and $^1\widetilde{f}_3 = 247$ Hz. It can be undoubtedly seen that the damage is located.

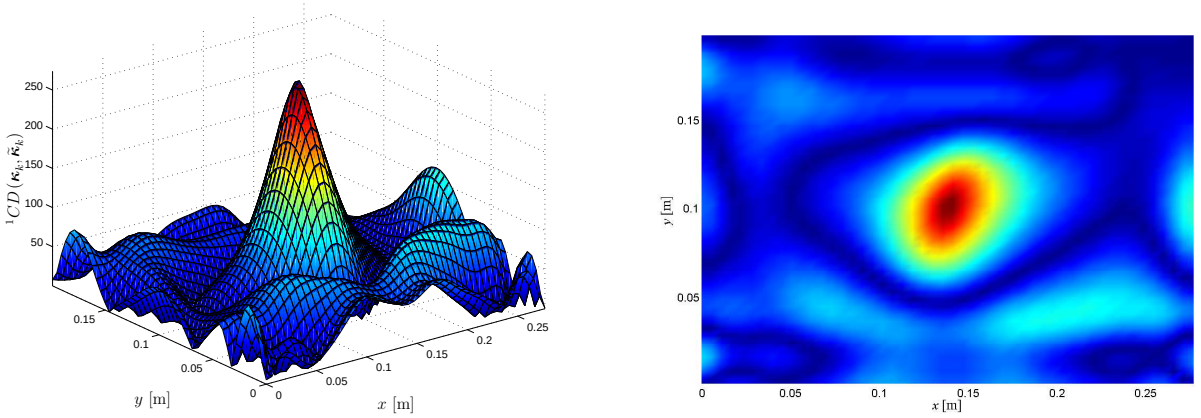

(a) 3D plot (b) Contour plot

Figure 11: Damage case 1 localization with Curvature Differences method and third mode ($f_3 = 248.0$ Hz).

For both damages, one in the plate center and the other on its upper right corner, the most changed mode is the sixth (see Table 3), to which correspond the undamaged and damage natural frequencies $f_3 = 440.5$ Hz and ${}^2\widetilde{f}_6 = 438.0$ Hz, respectively. The Curvature Differences method results, using only this mode shape curvature ($n = 1$ and $i = 6$ in expression (4)) are presented in a 3D plot and a contour plot in Figures 12(a) and 12(b). These Figures show the presence of damage in the plate upper right corner. However, the damage present in the plate center is not detected.

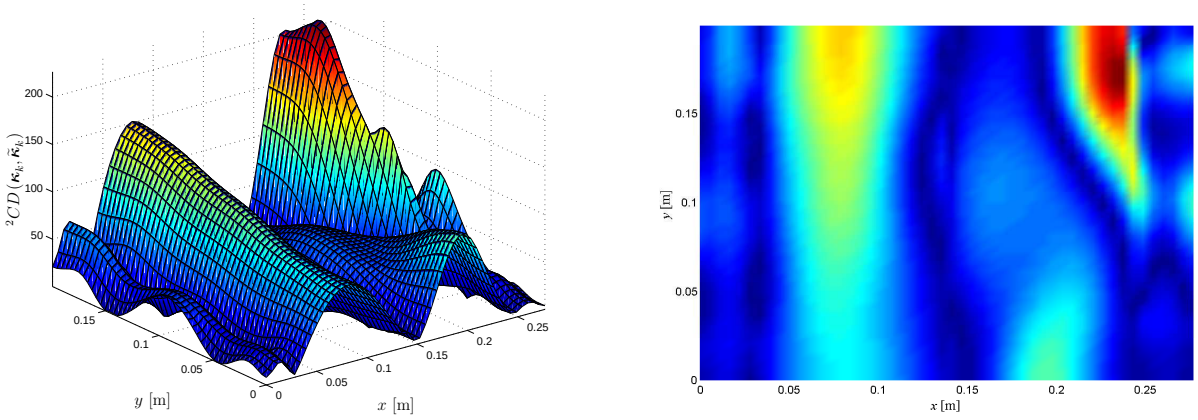

(a) 3D plot

(b) Contour plot

Figure 12: Damage case 2 localization with Curvature Differences method and sixth mode ($f_6 = 440.5$ Hz).

4.2 Other non destructive inspection methods

The damages inflicted to the plate are not detected by global visual inspection. Only by close examination is it possible to see some small indentations on the plate surface, where the impacts were made. The presence of damages was also not detected by standard X-ray inspections.

After both damages were inflicted to the plate, a C-Scan analysis was also performed. Figures 13(a) and 13(b) present the scanning results for all plate and for its center area, respectively. One notes that the damage in the center of the plate is detected, although the damage in the plate upper right corner is not. Since the damage in this area was inflicted by percussion with a hammer, the S-Can is unable to detect it.

5 CONCLUSIONS

In this paper is presented, applied and discussed three methods for damage localization of impact damage in laminated plates, based on mode shapes curvature differences. The mode shapes translations are experimentally obtained using double pulse-electronic holographic interferometry and a acoustic excitation. To overcome the problem of differentiating noisy data, the rotations and curvatures are obtained by applying a novel differentiation/smoothing technique. A carbon fiber reinforced epoxy rectangular plate, free in space, was subjected to two cases of impact damage. The results of applying the method showed that the curvature differences allows the damages localization. These damages can be undetected by visual, standard X-ray or C-Scan inspections. It was also found that the best localizations are achieved by selecting the most changed mode.

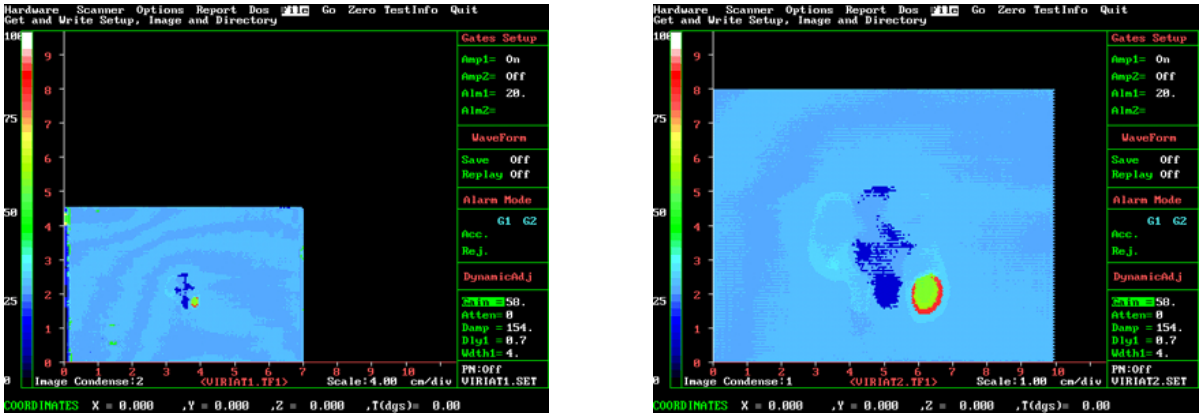

(a) C-scan of all plate (b) C-scan of plate center

Figure 13: C-Scan of plate with damage in center and upper right corner.

ACKNOWLEDGEMENTS

The authors greatly appreciate the financial support of FCT/POCTI/FEDER, FCT/POCTI (2010)/FEDER, Project POCTI/EME/56616/2004 and the EU through FP6-STREP Project Contract No. 013517-NMP3-CT-2005-0135717. The first author is most obliged to Prof. Luís Reis for preparing the laminated plate and to Mr. Manuel Bessa for performing the X-ray analysis.

REFERENCES

[1] S.W. Doebling, C.R. Farrar, M.B. Prime and D.W. Shevitz. *Damage identification and health monitoring of structural and mechanical systems from changes in their vibration characteristics: A literature review*. LA–13070–MS, Los Alamos National Laboratory, 1996.

[2] Y. Zou, L. Tong and G.P. Steven. Vibration-based model-dependent damage (delamination) identification and health monitoring for composites structures - a review, *Journal of Sound and Vibration*, **230(2)**, 357–378, 2000.

[3] M.A.-B. Abdo and M. Hori. A numerical study of structural damage detection using changes in the rotation of mode shapes, *Journal of Sound and Vibration*, **251(2)**, 227–239, 2002.

[4] A.K. Pandey, M. Biswas and M.M. Samman. Damage detection from changes in curvature mode shapes, *Journal of Sound and Vibration*, **145(2)**, 321–332, 1991.

[5] E. Sazonov and P. Klinkhachorn. Optimal spatial sampling interval for damage detection by curvature or strain energy mode shapes, *Journal of Sound and Vibration*, **285(4–5)**, 783–801, 2005.

[6] C. Reinsch C. This week's citation classic: Reinsch C H, smoothing by spline functions, *Current Contents/Engineering Technology & Applied Sciences*, **24**, 20, 1982.

[7] H.M.R. Lopes, R.M. Guedes and M.A. Vaz. An improved mixed numerical-experimental method for stress field calculation. *Optics & Laser Technology*, 2005 (Accepted for publication).

[8] J. Babaud, A.P. Witkin, M. Baudin and R.O. Duda. Uniqueness of the gaussian kernel for scale-space filtering, *IEEE Transactions on Pattern Analysis and Machine Intelligence*, **8(1)**, 26–33, 1986.

[9] J. Bevington and M. Mersereau. Diferential operator based edge and line detection, In: IEEE International Conference on ICASSP '87, Vol. 7, 249–252, 1987.

[10] C.A. Sciammarella and T.Y. Chang. Holographic interferometry applied to the solution of a shell problem, *Experimental Mechanics*, **14(6)**, 217–224, 1974.

[11] C.A. Sciammarella and S.K. Chawla. Lens holographic-moire technique to obtain components of displacements and derivatives, *Experimental Mechanics*, **18(10)**, 373–381, 1978.

[12] C.M.M. Mota Soares, M.M. Freitas, A.L. Araújo and P. Pedersen. Identification of material properties of composite plate specimens, *Composite Structures*, **25(1–4)**, 277–285, 1993.

[13] M. Takeda, H. Ina and S. Kobayashi. Fourier-transform method of fringe-pattern analysis for computer-based topography and interferometry, *Journal of the Optical Society of America*, **72(1)**, 156–160, 1982.

[14] J.A.G. Chousal. *Técnicas de processamento de imagens obtidas por métodos ópticos em análise experimental de tensões*, Ph.D. thesis, Faculdade de Engenharia da Universidade do Porto, Departamento de Engenharia Mecânica e Gestão Industrial, Porto, 1999 (In Portuguese).

[15] D.C. Ghiglia and M.D. Pritt. Two-Dimensional Phase Unwrapping: Theory, Algorithms, and Software, Wiley, New York, , Chap. xiv, p. 493, 1998.

[16] Q. Kemao. Windowed fourier transform for fringe pattern analysis, *Applied Optics*, **43(13)**, 2695–2702, 2004.

[17] Q. Kemao. Windowed fourier transform for fringe pattern analysis: Addendum, *Applied Optics*, **43(17)**, 3472–3473, 2004.

[18] G. Pedrini, B. Pfister and H. Tiziani. Double pulse-electronic speckle interferometry, *Journal of Modern Optics*, **40(1)**, 89–96, 1993.

[19] V.V. Volkov and Y.M. Zhu. Deterministic phase unwrapping in the presence of noise, *Optics Letters*, **28(22)**, 2156–2158, 2003.